Stable oxygen isotopes in Romanian oak tree rings record summer droughts and associated large-scale circulation patterns over Europe

Viorica Nagavciuc[1,2,3,4], Monica Ionita [5], Aurel Perșoiu [4,6], Ionel Popa[7], Neil J. Loader[8], Danny McCarroll[8]

[1]Faculty of Forestry, Ștefan cel Mare University, Suceava, Romania
[2]Institute for Geological and Geochemical Research, Research Centre for Astronomy and Earth Sciences, Hungarian Academy of Sciences, Budapest, Hungary
[3]Departement of Geography, Johannes Gutenberg University, Mainz, Germany
[4]Stable Isotope Laboratory, Ștefan cel Mare University, Suceava, Romania
[5]Paleoclimate Dynamics Group, Alfred-Wegener-Institute for Polar and Marine Research, Bussestrasse 24, Bremerhaven, D-27570, Germany
[6]Emil Racoviță Institute of Speleology, Romanian Academy, Cluj-Napoca, Romania
[7]National Research and Development Institute for Silviculture Marin Drăcea, Câmpulung Moldovenesc, Romania
[8]Department of Geography, College of Science, Swansea University, Singleton Park, Swansea SA2 8PP, UK

Correspondence to: nagavciuc.viorica@gmail.com

Abstract

We present the first annual oxygen isotope record (1900 – 2016) from the latewood (LW) cellulose of oak trees (*Quercus robur*) from NW Romania. As expected, the results correlate negatively with summer relative humidity, sunshine duration and precipitation and positively with summer maximum temperature. Spatial correlation analysis reveals a clear signal reflecting drought conditions at a European scale. Interannual variability is influenced by large-scale atmospheric circulation and by surface temperatures in the North Atlantic Ocean and the Mediterranean Sea. There is considerable potential to produce long and well-replicated oak tree ring stable isotope chronologies in Romania which would allow reconstructions of both regional drought and large-scale circulation variability over southern and central Europe.

Keywords
Oak, $\delta^{18}O$, Relative Humidity, Dendrochronology, Atmospheric circulation

1. Introduction

European droughts and heat waves have increased in frequency and intensity in the 21st century (van Lanen et al., 2016; Ionita et al., 2017, 2015), leading to increased risks to human health, property and infrastructure. Climate models suggest that rising global temperatures will lead to more frequent and stronger heat waves and summer droughts in the coming century, with southeastern Europe being particularly affected (Spinoni et al. 2015). The triggering mechanisms behind the genesis and dynamics of heat waves are complex (Kingston et al. 2015; Ionita et al. 2017), and existing observational data are insufficient to offer robust explanations. There is thus a need to look for alternative sources to reconstruct hydroclimatic variability on multi-centennial and longer timescales (Jones and Mann 2004; Huber and Gulledge 2011; Smerdon and Pollack 2016).

Tree rings are well established archives of paleoclimatic information, with the advantages of length, annual resolution, precise dating and varied geographical distribution (Schweingruber 1996). However, robust reconstructions of past climate based on measures of tree growth, such as ring width, are restricted to areas where growth is strongly limited by a single well-definable climatic controller. Typically this is summer temperature at high altitudes/latitudes (Popa and Kern 2009; Popa and Bouriaud 2013; Nechita et al. 2017) and precipitation or related hydroclimatic variables in very dry environments (Popa and Sidor 2010; Kern et al. 2012; Levanič et al. 2013; Árvai et al. 2018). Measures of tree ring density (Grudd 2008; Kłusek et al. 2015), and the related property of blue reflectance (McCarroll et al. 2002; Wilson et al. 2014), can provide even stronger climatic signals, but are limited to conifers. In contrast, the $^{18}O/^{16}O$ ratio in tree rings is not dependent on net growth, but acts as a passive monitor of environmental change (McCarroll and Loader 2004; Leavitt 2010; Gagen et al. 2011; Young et al. 2015), potentially providing paleoclimate information for regions that are not close to an ecological limit (Haupt et al. 2011; Labuhn et al. 2016). The $\delta^{18}O$ values in tree ring cellulose depend on the stable isotope composition of the water taken up by roots, evaporative enrichment in the leaves and on biological fractionation and isotopic exchange occurring during photosynthesis and cellulose formation (McCarroll and Loader 2004; Gessler et al. 2013; Treydte et al. 2014). The $\delta^{18}O$ values in soil water are directly influenced by those in precipitation, in turn controlled by atmospheric circulation patterns, condensation temperature, precipitation amount and relative humidity (Dansgaard 1964). The dominant control on the enrichment of leaf water in the heavy isotopes is the difference in vapour pressure of leaf air and ambient air, which is controlled by relative humidity (Gessler et al. 2013; Labuhn et al. 2016). Dry and hot climate conditions lead to an enrichment in ^{18}O due to evaporation, yielding higher $\delta^{18}O$ values in tree-ring cellulose (Labuhn et al. 2016). The dominant environmental signals in tree ring oxygen stable isotope ratios are thus the stable isotope

81 composition of precipitation and summer relative humidity (McCarroll and Loader 2004; Labuhn et
82 al. 2014; Young et al. 2015).
83 In terms of dendrochronological series, Romania has a high potential to develop a well-
84 replicated oak chronology covering almost the entire Holocene using the wood from the well-
85 preserved oak forests together with abundant archaeological and sub-fossil oak timbers (Rădoane et
86 al. 2015; Kern and Popa 2016; Nechita et al. 2017). This region is characterized by limited tree-
87 ring-based climate reconstructions (Luterbacher et al. 2016), because tree ring widths are poorly
88 correlated with climate (Nechita and Popa 2012; Nechita 2014). Strong paleoclimate
89 reconstructions from this part of south-eastern Europe, where Atlantic, Mediterranean and
90 Scandinavian climatic influences converge, would fill a clear gap in the paleoclimatic data network
91 of Europe.
92 This study aims to evaluate the potential of oxygen isotopes in oak tree rings from Romania
93 for producing long records of hydroclimate, including summer drought, and to assess whether the
94 local variations in stable oxygen isotope ratios are linked to large-scale atmospheric circulation
95 patterns over Europe.
96
97 **2. Data and methods**
98 **2.1 Study area and meteorological data**
99 The Nușfalău sampling site is situated in north-western Romania, (47.19 °N, 22.66 °E, 270
100 m above sea level, (Figure 1). The local climate is temperate-continental, with mild winters, hot,
101 dry summers and westerlies dominating the atmospheric circulation. Local meteorological data for
102 the period 1961–2013 CE are available from the Romanian Meteorological Administration station
103 Oradea (47.04 °N, 21.91 °E), 60 km west of the study site. The meteorological data includes:
104 maximum (T_{max}), mean (T_{mean}), minimum (T_{min}) and soil temperature (T_{soil}), sunshine duration (SS),
105 cloud cover (CC), relative humidity (RH), and precipitation amount (PP). Highest monthly
106 precipitation amounts occur in June (78.26 mm on average), and the highest maximum temperatures
107 are recorded in July (27.2 °C on average) and August (27.2 °C on average). Over the 1961–2013
108 period, the highest precipitation amount was recorded in June 1980 (178.56 mm), and the highest
109 monthly maximum temperature was recorded in July 2012 (32.07 °C). The lowest relative humidity
110 occurs throughout the summer months (June – 71.63 % and July – 69.60 %).
111
112 **2.2 Gridded climate data**
113 Gridded precipitation amount totals, T_{mean} and the self-calibrated Palmer Drought Severity
114 Index (scPDSI) covering 1901–2014 CE were extracted from the monthly CRU T.S. 4.01 dataset
115 (Harris et al. 2013), with a spatial resolution of 0.5°×0.5°. To investigate links with Northern

Commented [DM1]: Do July and August have the same mean?

Hemisphere atmospheric circulation we used the seasonal means of Geopotential Height at 500 mb (Z500), zonal wind (U500) and meridional wind (V500) at 500 mb from the Twentieth Century Reanalysis (V2) data set (NCEPv2; Whitaker et al. 2004; Compo et al. 2006, 2011) on a 2°×2° grid, for the period 1901–2014 CE. The vertically integrated water vapor transport (WVT) (Peixoto and Oort 1992) was calculated through zonal wind (u), meridional wind (v) and specific humidity (q), from the same data set. WVT vectors for latitude (ϕ) and longitude (λ) are defined as follows:

$$\vec{Q}(\lambda,\phi,t) = Q_\lambda \vec{i} + Q_\phi \vec{j} \qquad \text{eq. (1)}$$

Where zonal (Q_λ) and meridional (Q_Φ) components of Q are given by eq. (2):

$$Q_\lambda = \int_0^{p_0} qu\frac{dp}{g}$$
$$Q_\phi = \int_0^{p_0} qv\frac{dp}{g} \qquad \text{eq. (2)}$$

where q = specific humidity, u = zonal wind, v = meridional wind and p = pressure. The WVT is obtained by summation of water transport for all layers located between the Earth's surface and 300 hPa, above which the specific humidity in the Twentieth Century Reanalysis (V2) model is zero (Kalnay et al. 1996; Whitaker et al. 2004; Compo et al. 2006, 2011). For sea surface temperature we used the 1°×1° Hadley Centre Sea Ice and Sea Surface Temperature data set—HadISST (Rayner 2003).

2.3 Development of tree-ring chronologies and statistical methods

Two 5 mm increment cores were collected from each of ten oak trees (*Quercus robur* L.) in August 2016 at Nușfalău using standard dendrochronological sampling methods (Schweingruber 1988). One core per tree was fixed in a wooden support, polished, scanned and ring widths measured using the CDendro software, with a precision of 0.01 mm. Cross dating was performed and verified using COFECHA software (Holmes 1983). For stable isotope analysis, nine of the unmounted cores were manually dissected with a scalpel under magnification and the latewood (summer-wood) sections pooled into one sample. The earlywood is excluded, because in *Q. robur*, earlywood vessels are formed about 2-3 weeks before bud burst and are completed before full leaf expansion (Puchałka et al. 2017). Alpha-cellulose was extracted from latewood samples following the method of Boettger et al. (2007) and Loader et al. (1997) and homogenized using a Hielscher ultrasonic device (Laumer et al. 2009). For each sample, 0.30-0.35 mg of cellulose were packed in silver capsules, freeze-dried and pyrolyzed using a Thermo Scientific Flash High-Temperature Elemental Analyzer (HTEA) and isotope ratios were measured on the evolved CO_2 using a Delta V Advantage IRMS in the Stable Isotope Laboratory at Swansea University. Every tenth sample was

measured three times, the analytical error being less than 0.3 ‰. The results are expressed using the conventional δ (delta) notation in per mil (‰) relative to the Vienna Standard Mean Ocean Water (VSMOW) standard (Coplen 1994).

Linear correlations between $\delta^{18}O$ and local monthly and seasonal climate parameters were explored using the Treeclim R package (R Development Core Team 2010), with confidence intervals calculated using the bootstrap method. To identify connections with large-scale atmospheric circulation and North Atlantic Ocean sea surface temperature (SST), we constructed composite maps of Z500 and SST standardized anomalies for the summer season by selecting the years when the value of normalized time series of $\delta^{18}O$ values was >1 standard deviation (High) and <−1 standard deviation (Low), respectively. These thresholds were chosen as a compromise between the strength of the climate anomalies linked to $\delta^{18}O$ anomalies and the number of maps that satisfy this criterion. Further analysis has shown that the results are not sensitive to the exact threshold value used for the composite analysis (not shown). The significance of the composite maps is based on a standard t-test (confidence level 95 %).

3. Results and discussions

3.1 Local climate signal and links to regional patterns

As expected in samples from a temperate-continental region, the $\delta^{18}O$ values are significantly (95% significance level) and positively correlated with local summer (June-July-August, JJA) sunshine duration (r = 0.55) and maximum temperatures (r = 0.48) and significantly negatively correlated with summer cloud cover (r = -0.49) and precipitation amount (r = -0.51). The strongest correlation, however, is with the most direct control on oxygen isotope fractionation in the leaf, which is summer relative humidity (r = -0.67). The calibration model passes standard split-period verification statistics (NCR 2006), including Reduction of Error (RE) and Coefficient of Efficiency (CE) (Table 1), suggesting that the relationship is temporally stable, and the correlation is strong enough to justify a variance-scaled reconstruction, so that past extremes are not routinely underestimated (McCarroll 2015). Given the short meteorological data set, the calibration - validation approach is supported by the results of a bootstrap approach to verification with 95% confidence limits.

The spatial validity of the relationship between $\delta^{18}O$ ratio and summer precipitation, drought conditions and temperature was also analyzed, over the period 1901–2016. The $\delta^{18}O$ values record both local signals (Figure S1, Table 2) and signals at a European scale. Significant correlations with summer PP (Figure 3a) extend over a wide area, with negative correlations over the whole of southern and central Europe and positive correlations over Fennoscandia. A similar dipole-like structure in the correlation analysis is found for the summer scPDSI index. High $\delta^{18}O$ values are

associated with drought conditions over the central and the eastern part of Europe and wet conditions over Fennoscandia. The highest correlations are found over the eastern part of Europe (Figure 3b). Strong spatial field correlations are found also for summer maximum temperature (Figure 3c). High values of $\delta^{18}O$ are associated with hot summers over the whole of central and eastern Europe and cold summers over the northern part of Europe. The dipole-like structure identified in the correlation maps for PP and scPDSI is a well-known feature of summer hydroclimate at a European scale (Ionita et al. 2012; Ionita 2015). In general droughts and heat waves over the central and southern part of Europe are accompanied by prolonged wet and cold periods over the northern part of Europe, as in the summers of 1904, 1921, 1976 and 2015 (Ionita et al. 2012; Ionita 2015). This can be regarded as an indication that the $\delta^{18}O$ in tree rings for our site location is able to record not just dry/wet periods at a local scale, but is able to record also dry/wet periods at a European scale.

The highest correlation coefficients were found between $\delta^{18}O$ values and summer scPDSI field. As already indicated by the correlation analysis with local climate data (Table 2), $\delta^{18}O$ values are very sensitive to relative humidity and drought conditions. In order to better analyze the relationship between $\delta^{18}O$ and summer drought, a longer scPDSI series was extracted by averaging the gridded data over the region (20 °E–25 °E, 45 °N–50 °N). The temporal evolution of the $\delta^{18}O$ values and the scPDSI index is shown in Figure 4a. The correlation coefficient between the two-time series is $r = -0.52$ ($p<0.001$) and prolonged dry periods (e.g. 1941–1950) are always associated with high values of $\delta^{18}O$. A striking feature of the $\delta^{18}O$ record is that it captures all of the extremely dry years (1954, 1976, 2003 and 2015), which were characterized by prolonged and extended droughts at a European scale (Ionita 2015; Spinoni et al. 2015; Ionita et al. 2017). The good agreement between the $\delta^{18}O$ record and the scPDSI time series and the results of the calibration model (Table 2) thus indicate that $\delta^{18}O$ values can be used as a proxy for the occurrence of dry/wet condition, especially over the eastern part of Europe.

To further explore the scPDSI signal in the $\delta^{18}O$ chronology, we compare the probability distribution function of $\delta^{18}O$ values for dry (scPDSI < -2) and wet (scPDSI Index > 2) summers (Figure 4b). The +/-2 threshold was chosen to focus just on the years that are characterized by extreme droughts. Values between -2 and 2 for the scPDSI index indicate normal conditions, thus they are excluded from our analysis. The mean $\delta^{18}O$ value for the dry years (29.51 ‰) is significantly higher ($p<0.001$) than the mean $\delta^{18}O$ value corresponding to wet years (28.13 ‰).

3.2 Moisture signal in the $\delta^{18}O$ values

Figure 5 shows the $\delta^{18}O$ time series, the seasonal cycle for precipitation and the daily maximum temperature for the instrumental period 1961–2013. Years recording the highest $\delta^{18}O$

values (> 1 standard deviation) and the lowest $\delta^{18}O$ years ($\delta^{18}O$ < -1 standard deviation) (Figure 5a) were selected and used to calculate the seasonal cycle in precipitation (Figure 5b) and the daily maximum temperature (Figure 5c). The blue lines (Figure 5b) indicate the seasonal cycle for the years with high precipitation detected by low $\delta^{18}O$ values, while red lines show the seasonal cycle for years with low precipitation as detected by high $\delta^{18}O$ values (Table S1). The black lines indicate the seasonal cycle computed over the period 1971-2000. As it can be inferred from Figure 5b, wetter conditions than average (blue lines) are detected from May until August for the extreme low $\delta^{18}O$ values. In contrast, drier conditions (red lines) are detected from May to October in relationship with extreme high $\delta^{18}O$ values. For the daily maximum temperature (Figure 5c) blue lines indicate that these years exhibit low daily maximum temperatures from June to August as detected by low $\delta^{18}O$ values. Red lines indicate that warm conditions prevail from May to August for years with high $\delta^{18}O$ values. The seasonal cycle analysis, for the extreme $\delta^{18}O$ values, indicates that there is no shift in the seasonal cycle for the extreme values, but there is a change in the absolute values of the analyzed variables. For example, the precipitation amount for low $\delta^{18}O$ values in May, June, July and August is more than double that recorded during the years with high $\delta^{18}O$ values. This verifies that the $\delta^{18}O$ in tree rings is able to capture the occurrence of extreme summers in terms of precipitation amount and temperature.

3.3 Tree ring oxygen isotope ratios and large-scale atmospheric circulation

The variations in the $\delta^{18}O$ values of tree rings have two major drivers: the stable isotope composition of the water absorbed through the roots and the evaporative enrichment of this water at the leaf surface (Roden et al. 2000). As the absorbed water is derived ultimately from precipitation, and its stable isotope composition can be controlled, inter alia, by atmospheric circulation (e.g. Gat, 1996) we hypothesize that $\delta^{18}O$ of tree rings will be able to record the prevailing large-scale atmospheric circulation. In general, persistent dry (wet) conditions are associated with anticyclonic (cyclonic) circulation in summer, while the sea surface temperature at the moisture source delivered to NW Romania plays also an important role via the interaction with large-scale climatic or oceanic variability (Ionita et al. 2012; Schubert et al. 2014; Ionita 2015). To examine the relationship between $\delta^{18}O$ and large-scale atmospheric circulation we constructed composite maps using summer northern hemisphere geopotential height at 500mb (Z500) and the vertically integrated water vapor transport (WVT). We focus on those years when the standardized (z-scored) $\delta^{18}O$ > 1 standard deviation (High) and $\delta^{18}O$ < -1 standard deviation (Low). The years that were used for the composite maps are shown in Table S1.

Low $\delta^{18}O$ values are associated with a Rossby wave train in the Z500 field, characterized by a low-pressure system over Greenland, followed by a high-pressure system in the central-north

Atlantic Ocean, a low-pressure system located over the central part of Europe and a high-pressure system over Fennoscandia and western Russia (Figure 6a). This Rossby wave structure in the Z500 field enhances the advection of moisture from the Atlantic towards the central and eastern part of Europe (Figure 6b). The enhanced moisture transport towards Europe is driven by the low-pressure system centered over Europe. Enhanced moisture advection leads to higher amounts of precipitation over the central and eastern part of Europe, which in turn will lead to low $\delta^{18}O$ values (amount effect, Dansgaard, 1964). A similar pattern, in the Z500 field, is obtained when we compute the composite maps associated with wet summers, based on the scPDSI index (Figure S2a). Positive $\delta^{18}O$ values are recorded in association with a horse shoe-like block pattern with a low-pressure system over the central North Atlantic Ocean, a high-pressure system over the central part of Europe and a low-pressure system over western Russia (Figure 6c). The anomalous Z500 center over Europe suggest a dominant subsidence and adiabatic warming associated with reduced cloudiness, heatwaves and reduced precipitation. The horse shoe-like block deflects the Atlantic storm tracks towards Fennoscandia (Figure 6d). Warm summers and reduced precipitation will lead to $\delta^{18}O$ values (in agreement with the findings from Figure 5), resulting from both the temperature effect of the stable isotope composition of precipitation and the potential sub-cloud evaporation of falling raindrops in a dry atmosphere. Strong evaporative enrichment at the leaf surface (as expected during warm and dry spells) would further enrich the water in ^{18}O over ^{16}O and drive $\delta^{18}O$ to higher values. Dry summers, as defined by the scPDSI index, are also associated with a similar horse shoe-like blocking pattern in the Z500 field (Figure S2b). From a long-term perspective, the Rossby wave-like structure identified in Figure 6c was found to be associated with the occurrence of heat waves and extremely high summer temperatures over the central and eastern part of Europe (Ionita et al. 2017). This suggests that the inter-annual variability of our Romanian $\delta^{18}O$ record captures very well the spatial structure of a relatively typical large-scale climatological feature that produces droughts in the central and eastern part of Europe.

3.4 Tree ring oxygen isotope ratios and North Atlantic Ocean SST

Previous studies have emphasized the role of the Atlantic Ocean and the Mediterranean Sea SSTs in driving the occurrence of heat waves and droughts over the European region (Feudale and Shukla 2011; Ionita et al. 2012, 2017; Kingston et al. 2013; Ionita 2015). Following this line, significant correlations between $\delta^{18}O$ values and North Atlantic Ocean SST (Figure 7a) indicate possible connections between the moisture availability over the eastern part of Europe and conditions at remote ocean areas. Positive $\delta^{18}O$ values are associated with positive SST anomalies in the North Atlantic Ocean, in a band stretching from 20 °N to 40 °N, the Mediterranean region and the Black Sea and negative SST anomalies in the central Atlantic Ocean. A similar SST pattern

is found if we compute the correlation maps between the scPDSI index and the North Atlantic SST (Figure 7b). Overall, the structure of the SST anomalies in Figure 7 resembles the SST anomalies responsible for the occurrence of extreme drought events over the southern and eastern part of Europe (e.g. in 2003, 2015) (Van Lanen et al. 2016; Ionita et al. 2017). Ionita et al., (2017) have recently shown that warm Mediterranean SSTs have preceded and occurred concurrently with dry summers over most of the central and eastern part of Europe. In some particular years (e.g. summers of 2003 and 2015), extremely dry and hot summers over the central and eastern part of Europe, have occurred simultaneously with cold SST anomalies in the central Atlantic Ocean. In general, the North Atlantic Ocean SSTs anomalies can explain many features of the European droughts and heatwaves (Feudale and Shukla 2011). Mediterranean SSTs usually have an additional effect, with warm SST's acting to reduce the baroclinicity over the European region and reinforcing the blocking circulation. Altogether, when favorable phase conditions are met, both the large-scale atmospheric circulation and the SST act as a driver and/or precursor for the dry/wet conditions at a European scale. Overall, SST can modulate the tree ring cellulose $\delta^{18}O$ ratios by modulating the prevailing large-scale circulation and the occurrence of droughts and heatwaves. Thus, the local tree ring $\delta^{18}O$ variability can be explained, at least partially, via the ocean-atmosphere interaction.

4. Conclusions

The calibration and verification results demonstrate that $\delta^{18}O$ values of the latewood cellulose of oak trees from Romania are a very good proxy indicator for local summer relative humidity and could be used to provide a long record of summer droughts. Spatial correlation analysis reveals that the $\delta^{18}O$ values also contain information on atmospheric circulation at a European scale, characterized by a dipole structure: negative correlations with drought conditions over the central and the eastern part of Europe and positive correlations with wet conditions over Fennoscandia. The internal variability of $\delta^{18}O$ values relates to large-scale summer atmospheric circulation, with high $\delta^{18}O$ values associated with anticyclonic circulation, drought and heat waves over the central and eastern part of Europe. There is considerable potential to produce long and well-replicated oak tree ring stable isotope chronologies in Romania which would allow reconstructions of both regional drought and large-scale circulation variability over southern and central Europe.

Acknowledgments. The research leading to these results has received funding from EEA Financial Mechanism 2009 - 2014 under the project contract no CLIMFOR18SEE. M. Ionita was funded by the Helmholtz Climate Initiative REKLIM. NJL and DMcC acknowledge support from the UK NERC NE/P011527/1.

References

Árvai M, Morgós A, Kern Z (2018) Growth-climate relations and the enhancement of drought signals in pedunculate oak (Quercus robur L.) tree-ring chronology in Eastern Hungary. iForest - Biogeosciences and Forestry 11:267–274. doi: 10.3832/ifor2348-011

Beck W, Sanders TGM, Pofahl U (2013) CLIMTREG: Detecting temporal changes in climate–growth reactions – A computer program using intra-annual daily and yearly moving time intervals of variable width. Dendrochronologia 31:232–241. doi: http://dx.doi.org/10.1016/j.dendro.2013.02.003

Boettger T, Haupt M, Knller K, et al (2007) Wood Cellulose Preparation Methods and Mass Spectrometric Analyses of δ13C, δ18O, and Nonexchangeable δ2H Values in Cellulose, Sugar, and Starch: An Interlaboratory Comparison. Analytical Chemistry 79:4603–4612. doi: 10.1021/ac0700023

Compo GP, Whitaker JS, Sardeshmukh PD, et al (2011) The Twentieth Century Reanalysis Project. Quarterly Journal of the Royal Meteorological Society 137:1–28. doi: 10.1002/qj.776

Compo GP, Whitaker JS, Sardeshmukh PD (2006) Feasibility of a 100-year reanalysis using only surface pressure data. Bulletin of the American Meteorological Society 87:175–190. doi: 10.1175/BAMS-87-2-175

Coplen TB (1994) Reporting of stable hydrogen, carbon, and oxygen isotopic abundances. Pure and Applied Chemistry 66:273–276. doi: 10.1351/pac199466020273

Dansgaard W (1964) Stable isotopes in precipitation. Tellus. doi: 10.3402/tellusa.v16i4.8993

Feudale L, Shukla J (2011) Influence of sea surface temperature on the European heat wave of 2003 summer. Part II: a modeling study. Climate Dynamics 36:1705–1715. doi: 10.1007/s00382-010-0789-z

Gagen MH, Mccarroll D, Loader NJ, Robertson I (2011) Stable isotopes in dendroclimatology: moving beyond "Potential"

Gessler A, Brandes E, Keitel C, et al (2013) The oxygen isotope enrichment of leaf-exported assimilates - does it always reflect lamina leaf water enrichment? New Phytologist 200:144–157. doi: 10.1111/nph.12359

Grudd H (2008) Torneträsk tree-ring width and density AD 500–2004: a test of climatic sensitivity and a new 1500-year reconstruction of north Fennoscandian summers. Climate Dynamics 31:843–857. doi: 10.1007/s00382-007-0358-2

Harris I, Jones PD, Osborn TJ, Lister DH (2013) Updated high-resolution grids of monthly climatic observations – the CRU TS3 . 10 Dataset. International Journal of Climatology. doi: 10.1002/joc.3711

Haupt M, Weigl M, Grabner M, Boettger T (2011) A 400-year reconstruction of July relative air humidity for the Vienna region (eastern Austria) based on carbon and oxygen stable isotope ratios in tree-ring latewood cellulose of oaks (Quercus petraea Matt. Liebl.). Climatic Change 105:243–262. doi: 10.1007/s10584-010-9862-1

Huber DG, Gulledge J (2011) Extreme Weather and Climate Change Understanding the Link, Managing the Risk. Science and Impacts Program Center for Climate and Energy Solutions 1–13. doi: 10.1002/hyp.7574

Ionita M (2015) Interannual summer streamflow variability over Romania and its connection to large-scale atmospheric circulation. International Journal of Climatology 35:4186–4196. doi: 10.1002/joc.4278

Ionita M, Lohmann G, Rimbu N, et al (2012) Interannual to decadal summer drought variability over Europe and its relationship to global sea surface temperature. Climate Dynamics 38:363–377. doi: 10.1007/s00382-011-1028-y

Ionita M, Tallaksen LM, Kingston D, et al (2017) The European 2015 drought from a hydrological perspective. Hydrology and Earth System Sciences 21:1397–1419. doi: 10.5194/hess-21-3001-2017

Jones PD, Mann ME (2004) Climate over past millenia. Reviews of Geophysics 42:1–42. doi: 10.1029/2003RG000143.CONTENTS

Kalnay E, Kanamitsu M, Kistler R, et al (1996) NCAR 40-year reanalysis project. Bull Amer Meteor Soc 77 SRC-:437–470

Kern Z, Patkó M, Kázmér M, et al (2012) Multiple tree-ring proxies (earlywood width , latewood width and d 13 C) from. Quaternary International 1–11. doi: 10.1016/j.quaint.2012.05.037

Kern Z, Popa I (2016) Dendrochronological and radiocarbon analyses of subfossil oaks from the foothills. Geochronometria 43:113–120. doi: 10.1515/geochr-2015-0038

Kingston DG, Fleig AK, Tallaksen LM, Hannah DM (2013) Ocean–Atmosphere Forcing of Summer Streamflow Drought in Great Britain. Journal of Hydrometeorology 14:331–344. doi: 10.1175/JHM-D-11-0100.1

Kingston DG, Stagge JH, Tallaksen LM, Hannah DM (2015) European-scale drought: Understanding connections between atmospheric circulation and meteorological drought indices. Journal of Climate 28:505–516. doi: 10.1175/JCLI-D-14-00001.1

Kłusek M, Melvin TM, Grabner M (2015) Multi-century long density chronology of living and sub-fossil trees from Lake Schwarzensee, Austria. Dendrochronologia 33:42–53. doi: http://dx.doi.org/10.1016/j.dendro.2014.11.004

Labuhn I, Daux V, Girardclos O, et al (2016) French summer droughts since 1326 CE: A reconstruction based on tree ring cellulose δ18O. Clim Past 12:1101–1117. doi: doi:10.5194/cp-12-1101-2016

Labuhn I, Daux V, Pierre M, et al (2014) Tree age, site and climate controls on tree ring cellulose δ18O: A case study on oak trees from south-western France. Dendrochronologia 32:78–89. doi: doi:10.1016/j.dendro.2013.11.001

Laumer W, Andreu L, Helle G, et al (2009) A novel approach for the homogenization of cellulose to use micro-amounts for stable isotope analyses. Rapid Communications in Mass Spectrometry 23:1934–1940

Leavitt SW (2010) Tree-ring C–H–O isotope variability and sampling. Science of The Total Environment 408:5244–5253. doi: http://dx.doi.org/10.1016/j.scitotenv.2010.07.057

Levanič T, Popa I, Poljanšek S, Nechita C (2013) A 323-year long reconstruction of drought for SW Romania based on

black pine (Pinus nigra) tree-ring widths. International journal of biometeorology 57:703–714. doi: 10.1007/s00484-012-0596-9
Loader NJ, Robertson I, Barker a. C, et al (1997) An improved technique for the batch processing of small wholewood samples to α-cellulose. Chemical Geology 136:313–317. doi: 10.1016/S0009-2541(96)00133-7
Luterbacher J, Werner JP, Smerdon JE, et al (2016) European summer temperatures since Roman times. Environmental Research Letters 11:024001. doi: doi:10.1088/1748-9326/11/2/024001
McCarroll D (2015) "Study the past, if you would divine the future": A retrospective on measuring and understanding Quaternary climate change. Journal of Quaternary Science 30:154–187. doi: 10.1002/jqs.2775
McCarroll D, Loader NJ (2004) Stable isotopes in tree rings. Quaternary Science Reviews 23:771–801. doi: http://dx.doi.org/10.1016/j.quascirev.2003.06.017
McCarroll D, Pettigrew E, Luckman A, et al (2002) Blue reflectance provides a surrogate for latewood density of high-latitude pine tree rings. Arctic, antarctic, and alpine research 4:450–453
NCR (2006) Surface temperature reconstructions for the last 2,000 years. Washington, DC.
Nechita C (2014) The dendroclimatic signal in Quercus robur. Analele Univeristății din Oradea, Facultatea Protecția Mediului XXIII:509–516
Nechita C, Popa I (2012) The relationship between climate and radial growth for the Oak (Quercus robur L.) in the Western Plain of Romania. Carpathian Journal of Earth and Environmental Sciences 7:137–144
Nechita C, Popa I, Eggertsson Ó (2017) Climate response of oak (Quercus spp.), an evidence of a bioclimatic boundary induced by the Carpathians. Science of the Total Environment 599–600:1598–1607. doi: 10.1016/j.scitotenv.2017.05.118
Peixoto JP, Oort AH (1992) Physics of Climate. Springer, New York, USA
Popa I, Bouriaud O (2013) Reconstruction of summer temperatures in Eastern Carpathian Mountains (Rodna Mts, Romania) back to AD 1460 from tree-rings. International Journal of Climatology n/a-n/a. doi: 10.1002/joc.3730
Popa I, Kern Z (2009) Long-term summer temperature reconstruction inferred from tree ring records from the Eastern Carpathians. Climate Dynamics 32:1107–1117
Popa I, Sidor C (2010) Rețeua romaneasca de dendrocronologie RODENDRONET 1. Conifere. Editura Silvica
Puchałka R, Koprowski M, Gričar J, Przybylak R (2017) Does tree-ring formation follow leaf phenology in Pedunculate oak (Quercus robur L.)? European Journal of Forest Research 136:259–268. doi: 10.1007/s10342-017-1026-7
R Development Core Team (2010) R: A language an environment for statistical computing
Rădoane M, Nechita C, Chiriloaei F, et al (2015) Late Holocene fluvial activity and correlations with dendrochronology of subfossil trunks: Case studies of northeastern Romania. Geomorphology 239:142–159. doi: 10.1016/j.geomorph.2015.02.036
Rayner NA (2003) Global analyses of sea surface temperature, sea ice, and night marine air temperature since the late nineteenth century. Journal of Geophysical Research 108:4407. doi: 10.1029/2002JD002670
Roden J, Lin G, Ehleringer JR (2000) A mechanistic model for interpretation of hydrogen and oxygen isotope ratios in tree-ring cellulose. Geochimica et Cosmochimica Acta 64:21–35
Schubert SD, Wang H, Koster RD, et al (2014) Northern Eurasian heat waves and droughts. Journal of Climate 27:3169–3207. doi: 10.1175/JCLI-D-13-00360.1
Schweingruber F-H (1996) Tree Rings and Environment. Dendroecology. Swiss Federal Intitute of Forest, Snow and Landscape Research WSL/FNP, Birmensdorf
Schweingruber FH (1988) Tree Rings Basics and Applications of Dendrochronology
Smerdon JE, Pollack HN (2016) Reconstructing Earth's surface temperature over the past 2000 years: the science behind the headlines. Wiley Interdisciplinary Reviews: Climate Change 7:746–771. doi: 10.1002/wcc.418
Spinoni J, Lakatos M, Szentimrey T, et al (2015) Heat and cold waves trends in the Carpathian Region from 1961 to 2010. International Journal of Climatology 35:4197–4209. doi: 10.1002/joc.4279
Treydte K, Boda S, Graf Pannatier E, et al (2014) Seasonal transfer of oxygen isotopes from precipitation and soil to the tree ring: Source water versus needle water enrichment. New Phytologist 202:772–783. doi: 10.1111/nph.12741
Van Lanen HAJ, Laaha G, Kingston DG, et al (2016) Hydrology needed to manage droughts: the 2015 European case. Hydrological Processes 30:3097–3104. doi: 10.1002/hyp.10838
van Lanen RJ, Groenewoudt BJ, Spek T, Jansma E (2016) Route persistence. Modelling and quantifying historical route-network stability from the Roman period to early-modern times (AD 100–1600): a case study from the Netherlands. Archaeological and Anthropological Sciences. doi: 10.1007/s12520-016-0431-z
Whitaker JS, Compo GP, Wei X, Hamill TM (2004) Reanalysis before radiosondes using ensemble data assimilation. Bulletin of the American Meteorological Society 132:2983–2991. doi: 10.1175/1520-0493(2004)132<1190:RWRUED>2.0.CO;2
Wilson R, Rao R, Rydval M, et al (2014) Blue Intensity for dendroclimatology: The BC blues: Acase study from British Columbia, Canada. The Holocene 24:1428–1438. doi: 10.1177/09559683614544051
Young GHF, Loader NJ, McCarroll D, et al (2015) Oxygen stable isotope ratios from British oak tree-rings provide a strong and consistent record of past changes in summer rainfall. Climate Dynamics 45:3609–3622. doi: 10.1007/s00382-015-2559-4

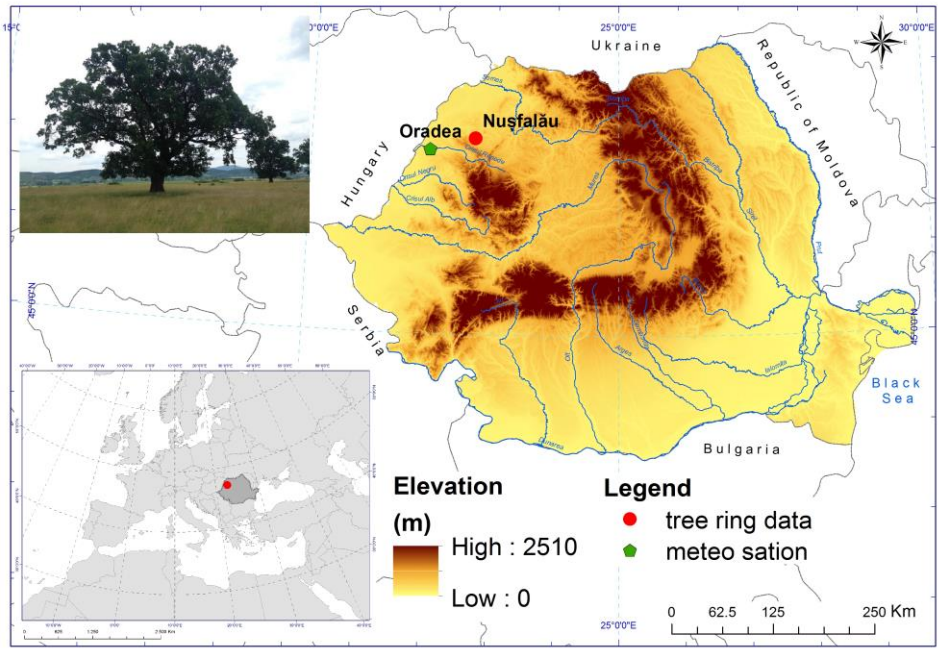

Figure 1. Location of the sampling site and the nearby meteorological station (Oradea), and an image of a typical oak tree in this area.

a)

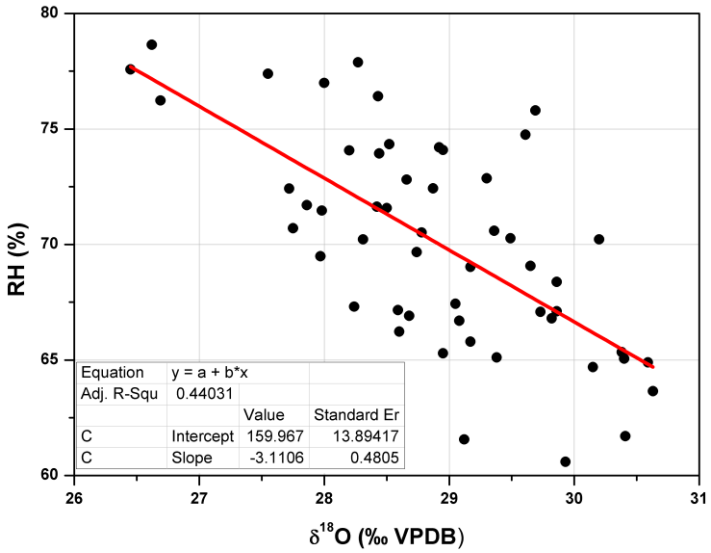

b)

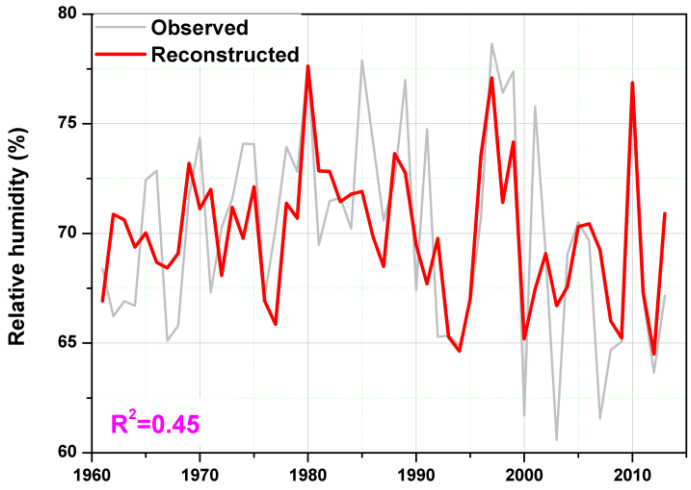

Figure 2. a) Regression of summer (JJA) relative humidity on $\delta^{18}O$ in the cellulose of late wood (LW) of oak tree-rings and b) Comparison between the observed (gray line) and the reconstruction (red line) mean summer relative humidity over the 1961 – 2013 period.

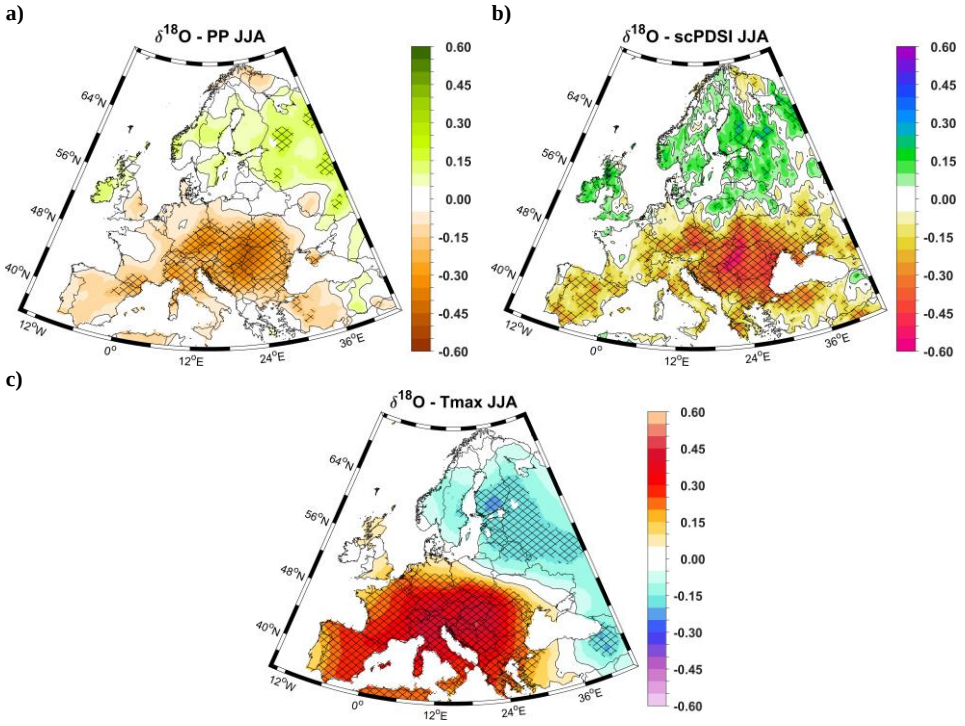

Figure 3. a) The spatial correlation map between $\delta^{18}O$ and: a) summer precipitation; b) summer scPDSI and c) summer Tmax. The hatching highlights significant correlation coefficients at a confidence level of 95%. Analyzed period: 1901 – 2014.

a)

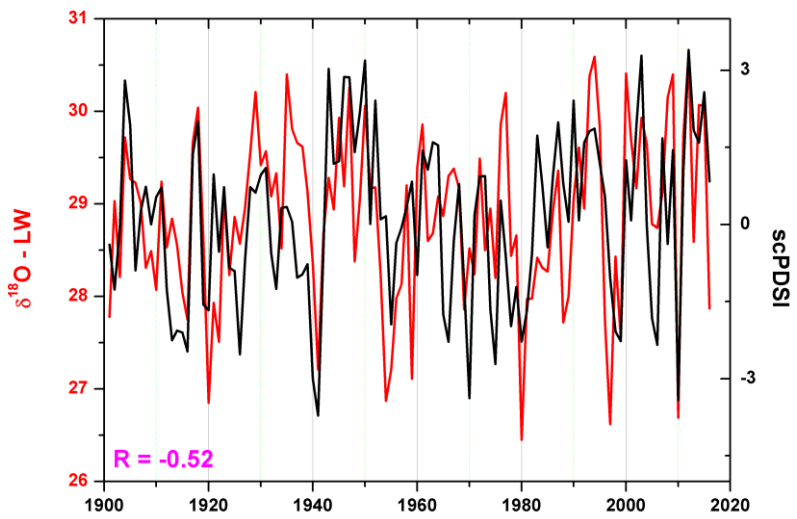

b)

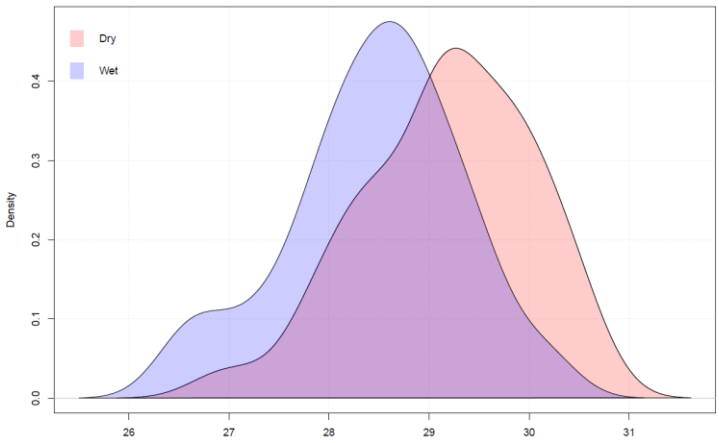

Figure 4. a) The temporal evolution of the $\delta^{18}O$ (red line) and the scPDSI index (black line) and b) changes in the $\delta^{18}O$ probability density function for dry years (scPDSI index < -2) and wet years (scPDSI index > 2). In a) the scPDSI index was multiplied by (-1) for a better comparison with the $\delta^{18}O$ time series.

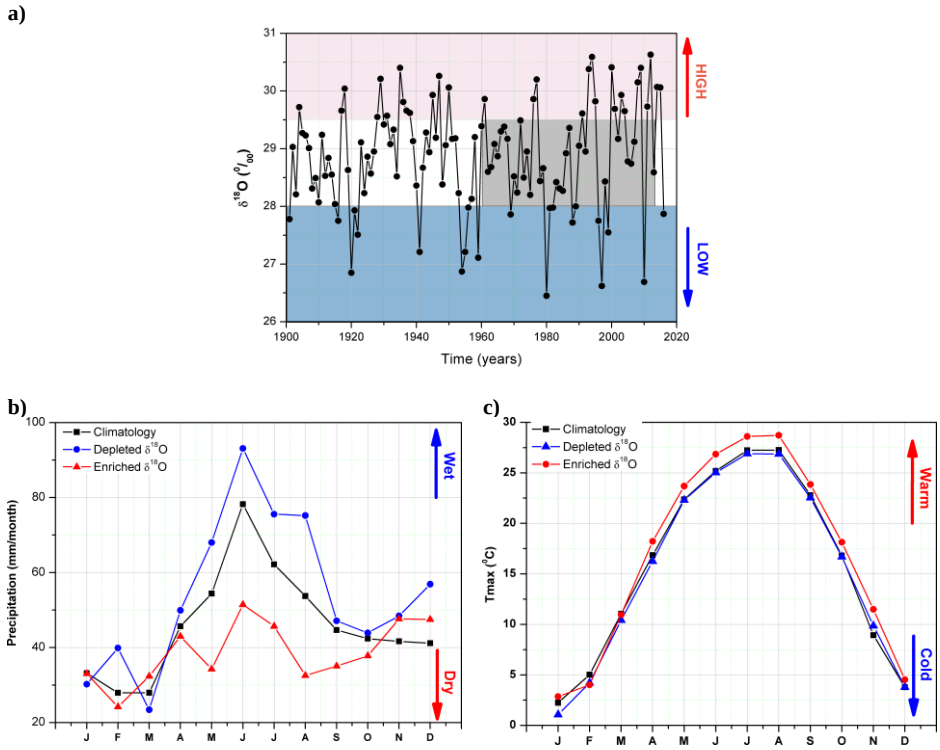

Figure 5. Analyzed period: 1961 – 2013.

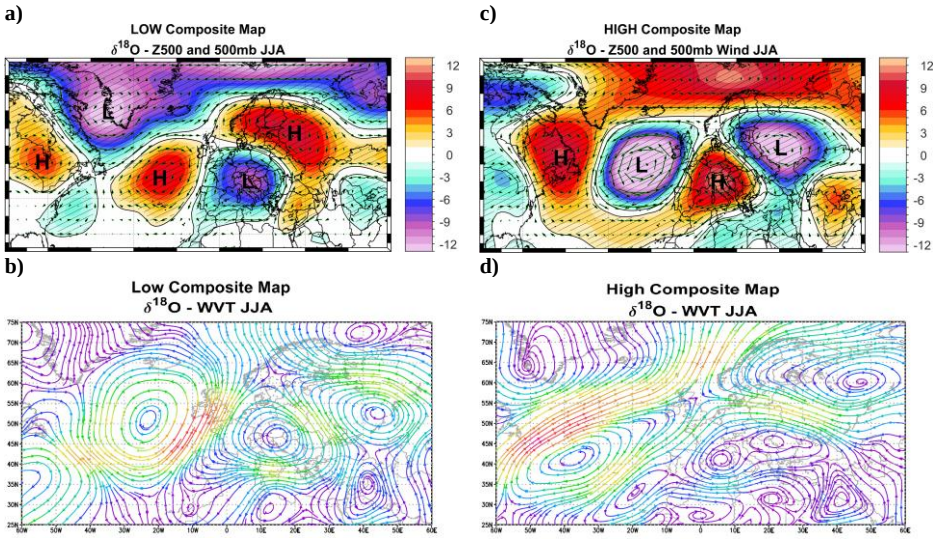

Figure 6. a) The composite map between Low $\delta^{18}O$ (< -1 std. dev.) and summer Geopotential Height at 500mb (Z500 – shaded areas) and summer 500mb Wind vectors (arrows); b) the composite map between Low $\delta^{18}O$ (< -1 std. dev.) and summer WVT; c) the composite map between High $\delta^{18}O$ (> 1 std. dev.) and summer Geopotential Height at 500mb (Z500 – shaded areas) and summer 500mb Wind vectors (arrows) and d) the composite map between High $\delta^{18}O$ (> 1 std. dev.) and summer WVT. The years used for the composite maps are shown in Table S1. Analyzed period: 1901 – 2014.

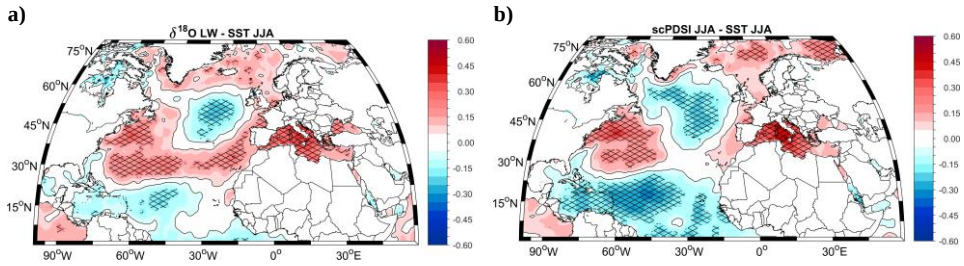

Figure 7. a) The correlation map between $\delta^{18}O$ LW and JJA SST and b) as in a) but for the summer scPDSI index. The hatching highlights significant correlation coefficients at a confidence level of 95%. Analyzed period: 1901 – 2014.

Table 1. Calibration and verification statistics between $\delta^{18}O$ and relative humidity in JJA.

Calibration	Verification	r	R^2	RE	CE
1961 - 1986		0.49	0.24		
	1986 - 2013	0.73	0.53	0.50	0.45
1987 - 2013		0.73	0.53		
	1961 - 1985	0.51	0.26	0.32	0.16
Full period		0.67	0.45		

r = correlation coefficient, R^2 = coefficient of determination, RE = reduction of error, CE = coefficient of efficiency.

Table 2. Calibration and verification statistics between $\delta^{18}O$ and scPDSI index in JJA.

Calibration	Verification	r	R^2	RE	CE
1901 - 1958		0.53			
	1959 - 2016	0.52	0.27	0.28	0.26
1959 - 2016		0.52			
	1901 - 1958	0.53	0.28	0.27	0.26
Full period		0.52	0.28		

r = correlation coefficient, R^2 = coefficient of determination, RE = reduction of error, CE = coefficient of efficiency.